SOLID STATE SYNTHESIS OF IRON(III) OXIDE POLYMORPHS FROM PRUSSIAN BLUE WITH DIFFERENT MORPHOLOGY

Claudia APARICIO*, Jiří TUČEK, Jan FILIP, Libor MACHALA

Regional Centre of Advanced Technologies and Materials (RCPTM),
Department of Experimental Physics, Faculty of Science, Palacky University,
Olomouc, Czech Republic, EU,
claudia.aparicio@upol.cz, jiri.tucek@upol.cz, jan.filip@upol.cz, libor.machala@upol.cz

Abstract

Two Prussian blue (PB) samples with different morphologies (spheres, mean size 160 nm; cubes, mean size 1.48 μm) and variable content of potassium (K-free and K-bearing) were used as a precursor material for the preparation of iron(III) oxides by solid state thermal decomposition method. A mixture of iron(III) oxide polymorphs (α-Fe_2O_3, β-Fe_2O_3, and γ-Fe_2O_3 nanoparticles) or pure maghemite (γ-Fe_2O_3 nanoparticles) were obtained by thermal decomposition of the cubic (K-bearing) or spherical (K-free) PB particles, respectively, at 350 °C in air. The particle's morphology of the starting material (i.e. PB) was mostly retained after the thermal decomposition. The PB samples and the as-formed iron(III) oxides were characterized by using X-ray powder diffraction (XRD), ^{57}Fe Mössbauer spectroscopy, and scanning electron microscopy (SEM). A high amount (50 wt%) of β-Fe_2O_3 polymorph was produced when K-bearing PB was used, simultaneously cubic clusters of maghemite were formed. A single phase (maghemite) clustered nanoparticles with spherical morphology were obtained when we used a K-free PB. The maghemite nanoparticles (4 nm) have proven to be superparamagnetic.

Keywords: Thermal decomposition, Prussian blue, iron oxides

1. INTRODUCTION

The control of size and morphology has been one of the main goals in the synthesis of nanoparticles. A variation of size and shape of nanoparticles leads to different optical, thermal, electrical, magnetic, and even catalytic properties of the materials [1,2]. Nanoparticles with defined shapes are usually synthesized by colloidal or thermal decomposition methods [1], using a suitable surfactant [3] or ultrasound during the synthesis [4]. It is also known that particle size have a direct effect on the decomposition temperature [1,5], also the morphology of particles might have a similar effect.

Iron(II) hexacyanoferrate ($Fe_4^{+3}[Fe^{2+}(CN)_6]_3 \cdot xH_2O$), also known as Prussian blue (PB) has been used as a precursor for iron oxides, prepared via solid state decomposition approach [6-8]. PB with different sizes and morphologies were used in those studies, including hollow particles [9], where in most of the cases the morphology and size of the precursor was maintained after the formation of iron oxides [8,9]. Generally, particles size [6] of a precursor and even the thickness of a layer [10] on the crucible affects the temperature of thermal decomposition and phase composition of iron oxide products as well. Another factor, which might influence the thermal behavior of the material and the formation of thermal decomposition products, is the particle's morphology of the precursor. The goal of the present work is to prepare iron oxides from Prussian blue, with emphasis on the influence of particle morphology on thermal decomposition of PB, and how it affects the shape of the resulting iron oxide particles.

2. MATERIALS AND METHODS

2.1. Synthesis of Prussian blue (PB)

Spherical particles of PB were prepared using the synthesis described by Shen et al. [3]. Polyvinylpyrrolidone (7.5 g, PVP, K-30, Mw = 40 000, Fluka) was dissolved in hydrochloric acid (100 ml, HCl, 0.01 M). Then, potassium hexacyanoferrate(III) (225 mg, $K_3[Fe(CN)_6]$, Lachema) was slowly added to the former solution under stirring. The resultant solution was refluxed at 80 °C for 2 hours, and afterwards centrifuged. The bright blue precipitate was dried in vacuum for 20 h, then powdered and labeled as PB-S.

Cubic particles of PB were synthesized using a sonochemical synthesis described by Wu et al. [4]. Potassium hexacyanoferrate(II) (423 mg, $K_4[Fe(CN)_3]\cdot 3H_2O$, Penta) was dissolved in hydrochloric acid (100 ml, HCl, 0.1 M). Then, the solution was immersed in an ultrasound bath at 40 °C for 4 hours. After that, the cooled solution was centrifuged. The dark blue precipitate was dried in air, powdered and labeled as PB-C.

2.2. Preparation of Iron(III) Oxides

The samples PB-S and PB-C (26 mg) were heated in a muffle furnace (Linn Hightherm Gmbh LM 112.07) from room temperature up to 350 °C in air (heating rate 5 °C/min); and then kept at 350 °C for 1 hour. The samples PB-C and PB-S, initially blue, changed color after heating to reddish brown color and dark brown color, respectively. The samples obtained after the heating were labeled as PBC350 and PBS350.

2.3. Samples Characterization

Simultaneous thermogravimetric analysis (TGA) and differential scanning calorimetry (DSC) were performed on PB-C and PB-S samples (10 mg of sample in an open alumina crucible) in air from 35 °C to 900 °C (heating rate 5 °C/min). The equipment used was a thermal analyzer STA 449 C Jupiter from Netzsch. After heating, samples were cooling down to room temperature under nitrogen.

X-ray powder diffraction (XRD) patterns were recorded with a PANalytical X'Pert PRO MPD diffractometer (Co-Kα radiation) in Bragg-Brentano geometry, equipped with an X'Celerator detector and programmable divergence and diffracted beam anti-scatter slits. Phase identification and Rietveld refinement were performed using the HighScore Plus software (PANalytical) in conjunction with PDF-4+ and ICSD databases.

Transmission ^{57}Fe Mössbauer spectroscopy was carried out in a constant acceleration mode using a ^{57}Co(Rh) source at room temperature (RT) and low temperatures (20 and 5 K). Spectra were folded and fitted using CONFIT2000 and Mosswinn software; the spectrometer was calibrated with a metallic α-iron foil.

Scanning electron microscopy (SEM) images of samples were obtained using a scanning electron microscope Hitachi SU-6600, with 5 kV and 15 kV setting. Complementary, energy dispersive X-ray analysis (EDS) was carried out as well on samples PB-C and PB-S.

3. RESULTS AND DISCUSSION

3.1. Prussian blue: Cubic and Spherical Shapes

XRD patterns and Mössbauer spectra confirm the presence of Prussian blue in both PB-S and PB-C samples (**Figure 1a, 1b**). From Mössbauer spectroscopy, the ratio Fe^{2+}/Fe^{3+} for samples PB-C (0.73) and PB-S (0.74) are very close to value 0.75 for stoichiometric Prussian blue. From SEM images (**Figure 1c**) is observed that particle sizes follow a normal distribution, with average sizes of 1.48 μm for cubic particles (PB-C) and 160 nm for spherical particles (PB-S). Moreover, EDS results (**Figure 1d**) show that both samples contain potassium in addition to the expected Fe, C, and N (N is overlapped by C contribution). PB-S sample contains only a negligible amount of K, where PB-C has a considerable amount of potassium.

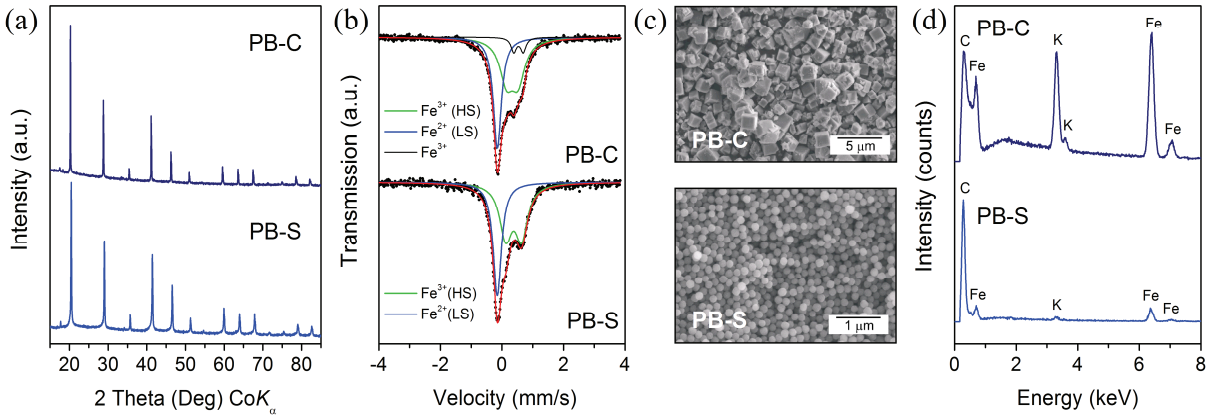

Figure 1 XRD patterns (a), RT Mössbauer spectra (b), SEM images (c), and EDS spectra (d) of cubic (PB-C) and spherical (PB-S) particles of Prussian blue.

3.2. Iron Oxide Formation after Heating of PB in Air

Above 250 °C, PB starts to decompose in air and the decomposition finishes after the total release of crystal water and cyanide groups from the lattice. There are visible differences in the TGA/DSC curves (**Figure 2**) for PB-S and PB-S. To explain the differences in thermal decomposition of PB, two structural models are used:

a) PB of spherical shape and without K in sample PB-S, $Fe_4[Fe(CN)_6]_3 \cdot xH_2O$ (space group *Pm*3*m*) with non-random distribution of vacancies [12];

b) PB of cubic shape and containing K in sample PB-C, $Fe_4[Fe(CN)_6]_3 \cdot [K^+_h \cdot OH^-_h \cdot mH_2O]$ (space group *Fm*3*m*), in this model we have coordinated water in a lattice with random vacancies of $[Fe^{2+}(CN)_6]^-$ units [11].

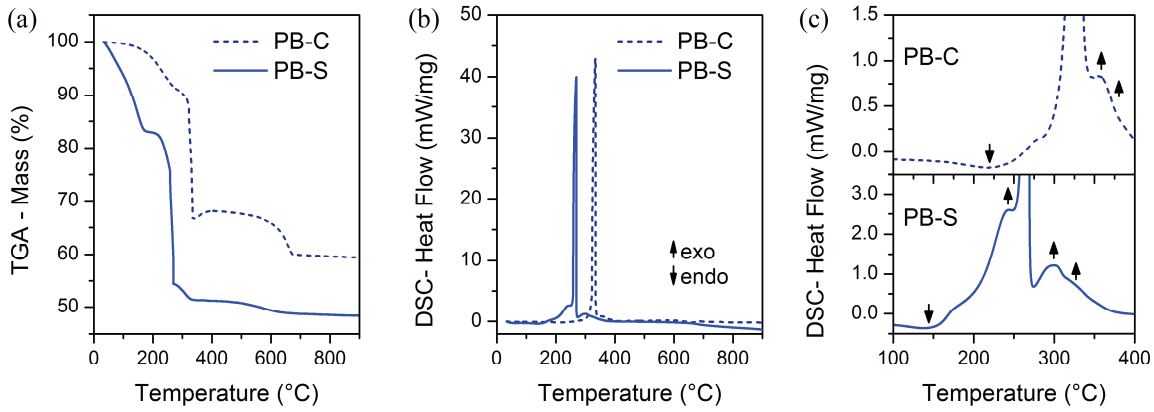

Figure 2 TG (a) and DSC (b) curves for PB-S (solid line) and PB-C (dashed line) samples. A detailed view of DSC curves (c), where the arrows represent endothermic (↓) and exothermic (↑) effects.

The differences in total mass loss (**Figure 2a**), for PB-S (-51.7 %) and PB-C (-40.6 %) are due to the different amount of water in the samples (9.5 in PB-S and 4.6 in PB-C) and the K presence in PB-C sample, where is expected the formation of KOCN and KNO_3 in addition to iron(III) oxides. Further heating above 400 °C leads to formation of hematite and potassium ferrite ($KFe_{11}O_{17}$), potassium ferrite was formed by the reaction between KNO_3 and Fe_2O_3. The position of exothermic peak on DSC curve (**Figure 2b**) is different for spherical particles (269 °C) in comparison with cubic particles (334 °C). Such a difference was observed previously by other authors in DSC curves of PB samples (K-free and K-bearing) with similar particles size (60 - 80 nm), where the main exothermal effect was reported at 260 °C for K-free PB and 278 °C for K-bearing

PB [12]. However, TGA performed on PB with bigger particles (150 - 200 nm) gave an exothermal effect slightly below 300 °C [7].

The proposed decomposition mechanisms are restricted only up to 400 °C (right after PB decomposition). Using the first model for PB-S, the equation (1) could explain the PB decomposition with the theoretical mass loss of 45.7 %, value just slightly smaller than the experimental one (48.6 %).

$$Fe_4[Fe(CN)_6]_3 \cdot 9.5\,H_2O + 5.25\,O_2 \rightarrow 3.5\,Fe_2O_3 + 9\,(CN)_2 + 9.5\,H_2O \quad (1)$$

After PB-C dehydration and release of cyanogen gas at 330 °C, iron(III) oxides and potassium cyanate (KOCN) are formed. In TG curve, between 335 and 400 °C (**Figure 2a**), the increment in mass (+1.5 %) accompanied by a small exothermal effect at 360 °C (**Figure 2c**) is explained by the decomposition of KOCN into KNO_3 and CO_2. Equation (2) summarizes the PB-C decomposition mechanism, where experimental (31.9 %) and theoretical (32.0 %) mass loss agree very well.

$$Fe_4[Fe(CN)_6]_3 \cdot K^+_{1.3}OH^-_{1.3} \cdot 4.6\,H_2O + 8.175\,O_2 \rightarrow 3.5\,Fe_2O_3 + 1.3\,KNO_3 + \ldots$$
$$\ldots + 8.35\,(CN)_2 + 5.25\,H_2O + 1.3\,CO_2 \quad (2)$$

3.3. Phase Composition and Morphology of the Iron(III) Oxide Samples

Despite the identical thermal treatment, the samples PBC350 and PBS350 differ significantly in phase composition. Sample PBC350 contained hematite (12 wt%), maghemite (38 wt%) and β-Fe2O3 (50 wt%), while only maghemite was found in sample PBS350 (**Figure 3a, 3b**). The RT Mössbauer spectra of samples PBC350 and PBS350 (**Figure 3c, 3d**) are similar; the Mössbauer parameters for both samples are listed in **Table 1**. In sample PBC350, the values of sub-spectral areas reveal that the dominant phase is β-Fe_2O_3 (58.7 %), followed by maghemite (34.2 %), and hematite (7.2 %).

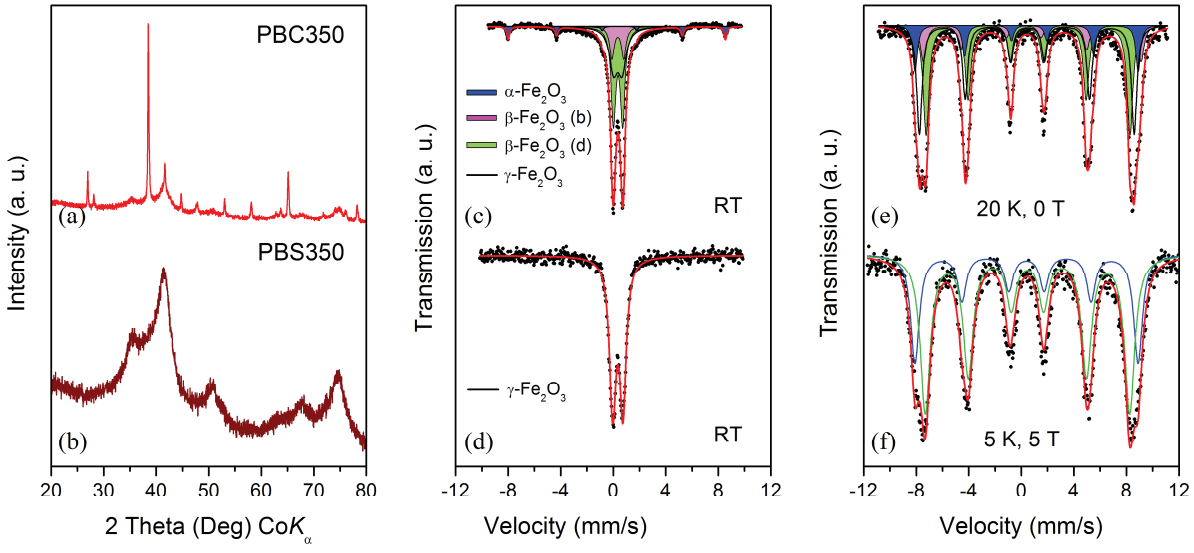

Figure 3 XRD patterns of the samples PBC350 (a) and PBS350 (b).
Mössbauer spectra for samples PBC350 (c, e) and PBS350 (d, f).

Low temperature Mössbauer spectra confirmed the presence of maghemite in both samples (**Figures 3e, 3f**). The ratio of ferric ions in O and T sites ($[Fe^{3+}]_O/[Fe^{3+}]_T$), in Mössbauer spectrum of PBS350 (**Figure 3f**), was determined as 1.67, which correspond to stoichiometric maghemite with vacancies only in octahedral sites. Using the relationship $\theta_c = arcsin[sqrt(6r/(4+3r))]$ (where: $r = A_{2,5}/A_{1,6}$; $A_{i,j}$ line intensity of line *i* or *j* of a sextet)

it was calculated the canting angle of spins for each sub-lattice of maghemite: $\theta_{c,A}$ = 44.6° (tetrahedral site) and $\theta_{c,B}$ = 59.0° (octahedral site) [13].

Table 1 Mössbauer parameters of samples PBC350 and PBS350. IS: isomer shift (± 0.01), QS: quadrupole splitting or quadrupole shift (± 0.01), W: line width (± 0.01), B_{hf}: magnetic hyperfine field or effective magnetic field[a] (± 0.1), Area (± 1.0), SP: superparamagnetism, WF: weak-ferromagnetism.

Sample	T (K)	Phase	IS (mm/s)	QS (mm/s)	W (mm/s)	B_{hf} (T)	Area (%)
PBC350	298	β-Fe_2O_3 b	0.35	0.90	0.41	-	15
		β-Fe_2O_3 d	0.37	0.70	0.41	-	44
		γ-Fe_2O_3 SP	0.35	0.65	0.75	-	34
		α-Fe_2O_3 WF	0.37	-0.20	0.25	51.4	7
PBS350	298	γ-Fe_2O_3 SP	0.35	0.77	0.59	-	100
PBC350	20	β-Fe_2O_3 b	0.51	0.64	0.53	51.5	13
		β-Fe_2O_3 d	0.48	0.07	0.53	48.2	39
		α-Fe_2O_3 WF	0.50	-0.20	0.41	52.8	13
		γ-Fe_2O_3	0.44	-0.05	0.48	50.8	35
PBS350	5	γ-Fe_2O_3 O	0.47	0.00	0.91	48.3[a]	62.5
	(5 T)	γ-Fe_2O_3 T	0.40	0.00	0.89	52.6[a]	37.5

The morphology of the iron(III) oxide samples vary depending on the PB precursor morphology, as can be observed from SEM images (**Figure 4**). When the particles of PB are spherical, the maghemite form spherical clusters (**Figure 4a**) with a smaller size than the PB-S precursor (116 nm). In the case of cubic PB particles, the maghemite forms cubic clusters with similar sizes as the PB-C precursor particles (**Figure 4b**). The preservation of the morphology during thermal transformation was addressed in previous works [7-9]. Maghemite clusters - cubic and spherical - are formed by small nanoparticles (4 nm, based on XRD). Because of their reduced sizes, each particle behaves as a single magnetic domain, and at room temperature they exhibit superparamagnetism, as confirmed by Mössbauer spectroscopy.

The β-Fe_2O_3 particles in PBC350, have a mean size of 70 nm (**Figure 4c**), similar to the estimated crystallite size (68 nm) from XRD. The β-Fe_2O_3 particles grow on the cubic cluster surfaces where the surface energy permits the polymorph transformation from γ- to β- ferric oxide.

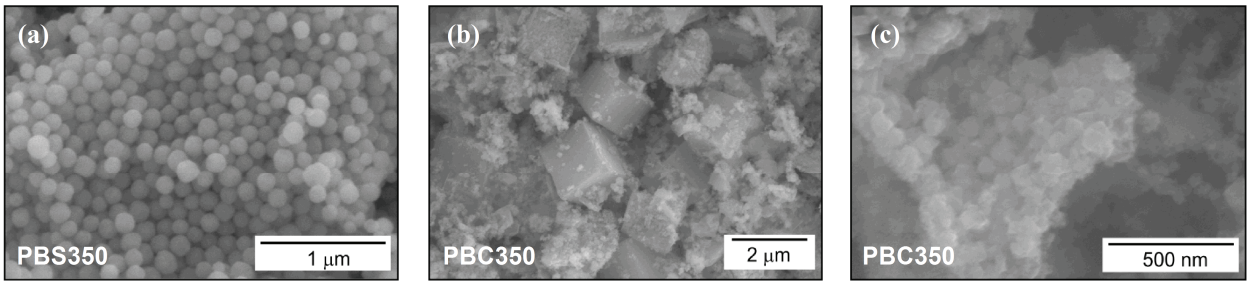

Figure 4 SEM images of the samples PBS350 (a) and PBC350 (b, c) showing the clusters of γ-Fe_2O_3 (b) and β-Fe_2O_3 nanoparticles (c)

4. CONCLUSION

The Prussian blue with two different morphologies (cubic and spherical) decomposes above 250 °C in air. At the beginning of the thermal decomposition of both PB samples (with and without K), after the initial dehydration and release of CN^- units, amorphous iron oxides are first formed, afterwards when the temperature

increases above 350 °C the amorphous iron oxides crystallize into γ-Fe_2O_3 or a mixture of α-Fe_2O_3, β-Fe_2O_3,and γ-Fe_2O_3 polymorphs. The maghemite (γ-Fe_2O_3) is in the form of clusters-forming nanoparticles (4 nm) retaining the original shape of the original precursor. Both maghemite clusters behave as superparamagnets at room temperature, making then interesting for potential applications. Finally, the differences in the TG and DSC curves for PB-C and PB-S are more likely due to a combined effect of the presence of potassium and particle sizes and not because of the particle's morphology.

ACKNOWLEDGEMENTS

The authors gratefully acknowledge the support by the project LO1305 of the Ministry of Education, Youth and Sports of the Czech Republic).

REFERENCES

[1] BURDA, Clemens, CHEN, Xiaobo, NARAYANAN, Radha and EL-SAYED, Mostafa A. Chemistry and properties of nanocrystals of different shapes. *Chemical Reviews*. 2005. 105, pp. 1025-102.

[2] XIA, Younan, XIONG, Yujie, LIM, Byungkwon and SKRABALAK, Sara E. Shape-Controlled Synthesis of Metal Nanocrystals: Simple Chemistry Meets Complex Physics? *Angewandte Chemie International Edition.* 2009. 48, pp. 60-103.

[3] SHEN, Xiaoping, WU, Shikui, LIU, Yan, WANG, Kun, XU, Zheng and LIU, Wei. Morphology Synthesis and Properties of Well-Defined Prussian Blue Nanocrystals by a Facile Solution Approach. *Journal of Colloid and Interface Science.* 2009. 329, pp. 188-95.

[4] WU, Xinglong, CAO, Minhua, HU, Changwen and HE, Xiaoyan. Sonochemical Synthesis of Prussian Blue Nanocubes from a Single-Source Precursor. *Crystal Growth & Design*. 2006. 6, pp. 26-28.

[5] REYES-LABARTA, Juan A. and MARCILLA Antonio. Kinetic Study of the Decompositions Involved in the Thermal Degradation of Commercial Azodicarbonamide. *Journal of Applied Polymer Science*. 2007. 107, pp. 339-346.

[6] MACHALA, Libor, ZOPPELLARO, Giorgio, TUČEK, Jiří, ŠAFÁŘOVÁ, Klára, MARUŠÁK, Zdeněk, FILIP, Jan, PECHOUŠEK, Jiří and ZBORIL, Radek. Thermal Decomposition of Prussian Blue Microcrystals and Nanocrystals Iron(III) Oxide Polymorphism Control Through Reactant Particle Size. *RSC Advances*. 2013. 3, pp. 19591-19599.

[7] ZHANG, Lei, BIN WU, Hao, XU, Rong and LOU, Xiong Wen (David). Porous Fe_2O_3 Nanocubes Derived from MOFS for Highly Reversible Lithium Storage. *CrystEngComm*. 2013. 15, pp. 9332-9335.

[8] ZAKARIA, Mohamed B., HU, Ming, HAYASHI, Naoaki, TSUJIMOTO, Yoshihiro, ISHIHARA, Shinsuke, IMURA, Masataka, SUZUKI, Norihiro, HUANG, Yu-Yuan, SAKKA, Yoshio, ARIGA, Katsuhiko, WU, Kevin C.-W. and YAMAUCHI, Yusuke. Thermal Conversion of Hollow Prussian Blue Nanoparticles into Nanoporous Iron Oxides with Crystallized Hematite Phase. *European Journal of Inorganic Chemistry*. 2014. 2014, pp. 1137-1141.

[9] ZHANG, Lei, WU, Hao Bin and LOU, Xiong Wen (David). Metal-Organic-Frameworks-Derived General Formation of Hollow Structures with High Complexity. *Journal of the American Chemical Society*. 2013. 135, pp. 10664-10672.

[10] HERMANEK, Martin and ZBORIL, Radek. Polymorphous Exhibitions of Iron(III) Oxide During Isothermal Oxidative Decompositions of Iron Salts: A Key Role of the Powder Layer Thickness. *Chemistry of Materials*.2008. 20, pp. 5284-5295.

[11] BUENO, Paulo R., FERREIRA, Fabio F., GIMÉNEZ-ROMERO, David, SETTI, Grazielle O., Setti, FARIA, Ronaldo C., GABRIELLI, Claude, PERROT, Hubert, GARCIA-JAREÑO, Juan J. and VICENTE, Francisco. Synchrotron Structural Characterization of Electrochemically Synthetized Hexacyanoferrates Containing K^+: A Revisited Analysis of Eletrochemical Redox. *The Journal of Physical Chemistry C*. 2008. 112, pp. 13264-13271.

[12] SAMAIN, Louise, GRANDJEAN, Fernande, LONG, Gary J., MARTINETTO, Pauline, BORDET, Pierre and STRIVAY, David. Relationship Between the Synthesis of Prussian Blue Pigments, Their Color, Physical Properties, and Their Behavior in Paint Layers. *The Journal of Physical Chemistry C*. 2013. 117, pp. 9693-9712.

[13] TUČEK, Jiří, ZBORIL, Radek and PETRIDIS, Dimitris. Maghemite Nanoparticles by View of Mössbauer Spectroscopy. *Journal of Nanoscience and Nanotechnology*. 2006. 6, pp. 926-947.